Proceedings 10th NUMGE 2023
10th European Conference on Numerical Methods in Geotechnical Engineering
Zdravkovic L, Kontoe S, Taborda DMG, Tsiampousi A (eds)

https://doi.org/10.53243/NUMGE2023-118

Numerical modelling of stone columns installation in clay

M. Miranda[1], A. Geramian[2], J. Castro[3], M. Ghazavi[4]

[1 3] *Department of Ground Engineering and Materials Science, Universidad de Cantabria, Santander, Spain*
[2 4] *Faculty of Civil Engineering, K. N. Toosi University of Technology, Tehran, Iran*

ABSTRACT: Installation effects of stone columns in purely cohesive soils are analysed using a Coupled Eulerian Lagrangian formulation in three-dimensions (3D). The installation process is simplified to the inclusion of rigid cylindrical elements with conical tips pushed into a single homogeneous soil layer with constant undrained shear strength. Dynamic effects, gravel placement and dissipation of excess pore pressures are not modelled. Tresca plasticity and a quasi-incompressible elastic law are used in the analyses. Installation of one single column, two columns and a group of nine columns are simulated to study the interaction between them. Results show the increase in radial stresses and pore pressures in the area close to the column, where the soil has been affected. When more than one column is modelled, the installation effects interact between each other, producing slightly higher radial stresses and pore pressures in a larger area. The peak of radial stresses appears a bit further away from the column in these cases.

Keywords: Stone columns; installation, radial stress, finite element analysis, Coupled Eulerian Lagrangian formulation

1 INTRODUCTION

Stone columns are commonly used in geotechnical practice to improve soils such as soft clays (e.g., Barksdale and Bachus 1983; Han 2015). They are vertical inclusions filled with gravel and their main effects are: improvement of bearing capacity, reduction of total and differential settlements, acceleration of consolidation and reduction the liquefaction potential. The most common construction methods are vibro-replacement and vibro-displacement depending on how the vibrator is pushed down with the aid of water or air, respectively (e.g., Kirsch and Kirsch 2010). They are frequently constructed using a vibrator that penetrates the ground and compacts the gravel from the bottom upwards. The installation of one column does not usually take a long time as it can be constructed in 15 to 30 minutes approximately; thus, in clayey soils it is a short time process and can be treated as an undrained situation. Field measurements have shown that the installation of the columns alters the properties of the native soil, such as increments in pore water pressures as well as in horizontal stresses (e.g., Kirsch 2004; Castro and Sagaseta 2012; McCabe et al. 2013; Amoroso et al. 2015). Hence, for an accurate design, it is important to account for these installation effects.

Stone columns are commonly constructed in small or large groups with distances between them of around 2 meters (area replacement ratios between 15 and 30%). Therefore, the effects of installation of the columns interact with each other and the installation sequence influences the soil alterations, as in the case of installation of rigid inclusions and piles (e.g., Nguyen et al. 2019; Soleimani and Weissenfels 2021). Numerical modelling has been used to study installation effects of stone columns. Most studies have simulated the installation of one single column through the simplification of cavity expansion in axial symmetry (e.g., Castro and Karstunen 2010; Sexton and McCabe 2015; Nagula et al. 2018). However, other approaches, such as the press-replace method or large displacement formulations, have also been used (e.g., Farias et al. 2005; Wang and Li 2019), but still mainly for single columns or piles. Modelling the installation effects of several stone columns have just been performed under oversimplifying assumptions (e.g., Kirsch 2006; Ellouze et al. 2017; Al Ammari and Clarke 2018).

Recently, the authors (Geramian et al. 2022) presented numerical simulations of the installation effects of a group of 9 stone columns to study the interaction between them using 3D Coupled Eulerian Lagrangian (CEL) finite element simulations. In this paper, these results and some salient features are further discussed. Section 2 presents again the numerical model to make this paper self-sufficient. Next, some of the numerical results are presented and discussed (Section 3). Finally, some conclusions are summarized.

2 NUMERICAL MODEL

Since stone column installation is a complex process, where large displacements take place, updated Lagrangian formulations are usually employed to account for them. In this study, the Coupled Eulerian Lagrangian

(CEL) formulation was implemented in the finite element code ABAQUS/Explicit to develop the numerical model (Figure 1). CEL is able to overcome mesh distortion problems because it combines the advantages of the Lagrangian and the Eulerian formulations. Each node of the Lagrangian mesh moves together with the material during the simulation, and each Lagrangian element is always associated with one type of material. Thus, the elements are deformed during the simulation. On the other hand, the nodes of a Eulerian mesh are fixed during the simulation, so that the elements cannot deform and the material flows through the Eulerian mesh. Therefore, a Eulerian element is not only dedicated to one type of material and may be "void" or not fully "filled". The CEL method allows an interaction between Lagrangian elements and Eulerian material through a contact formulation (further details may be found, for example, in Pucker and Grabe 2012).

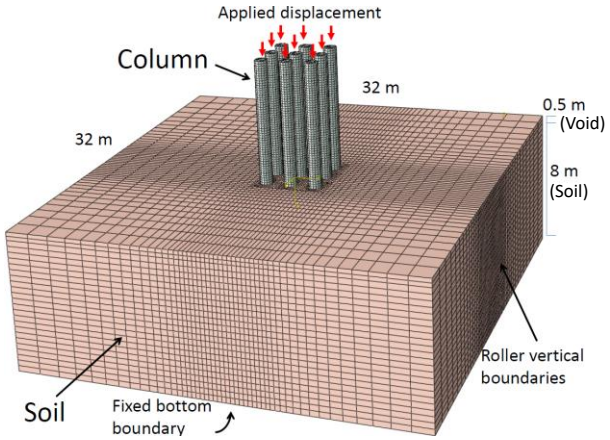

Figure 1. Numerical model and finite element mesh

The stone column installations have been simplified to the quasi-static insertions of rigid cylindrical elements to reduce the computational cost. Besides, lateral expansion is the main effect of column installation in clays (e.g., Castro and Karstunen 2010). The diameter of the cylindrical elements has been fixed as 1 m (radius R=0.5m) and Lagrangian elements were used for the cylinder mesh. Columns have been installed following a square pattern with an axis-to-axis distance of 2 m. This distribution results in an area replacement ratio of 19.6%. The tip of the cylindrical elements has been chosen as conical with a cone angle of 90º which represents the usual for deep vibrators (e.g., Kirsch and Kirsch 2010). The height of the tip is the same as the height of the upper 0.5-thick "void" layer (Eulerian mesh as detailed below). The tip of the cylindrical element before the installation is just place on top of the soil surface. The soil is formed by a homogeneous 8 m thickness soft soil layer resting on a rigid bedrock and divided into Eulerian elements. The width of the model was set to 32 m to avoid the influence of the lateral boundaries set as rollers (Figure 1). The columns fully penetrate the soft soil layer ("end-bearing" columns).

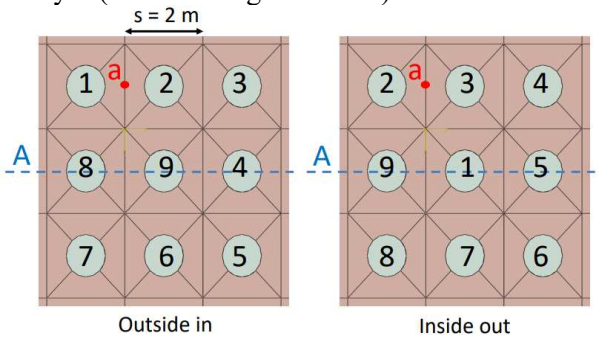

Figure 2. Installation sequences. Reference point and cross-section

The specific position of the ground water table was not considered. Lateral earth pressure coefficient was set at 0.8, which is equivalent to setting the ground water table at the surface and a K_0 =0.6. The soft soil is modelled by a quasi-incompressible elastic law and using Tresca plasticity. Common soft soil parameters are used (Table 1). This criterion was modelled in ABAQUS using the "Mohr-Coulomb" constitutive model with a negligible friction angle, namely 0.1.

Table 1 Soil properties

Soil property	*Value*	*Units*
Mass bulk density (ρ)	2,000	kg/m^3
Undrained shear strength (c_u)	30	kPa
Undrained Young's modulus (E_u)	3,000	kPa
Undrained Poisson's ratio (v_u)	0.495	
Earth pressure coefficient at rest (K_0)	0.6/0.8	
Henkel's a pore pressure parameter	0.3	
Skempton's A pore pressure parameter	0.75	

Numerical simulations first calculate the initial stress state. Next the cylindrical elements are pushed into the soil until they reach the rigid bedrock (the bottom boundary). Different configurations are analysed; first just the installation of one single column, followed by two columns and then a group of nine columns. In the latter case, two different installation sequences have been analysed one where the first column is in one corner of the mesh (named "outside in") and the other where the initial column is on the centre (named "inside out") (Figure 2).

3 RESULTS AND DISCUSSION

3.1 Single column installation

This case of one single column installation is set as the reference case for installation of a group of columns. The radial stress contours when the tip of the vibrator is at a depth of 4 meters are in Figure 3. As expected, and

presented by previous studies (e.g., Pucker and Grabe 2012) the radial stress increases around the tip.

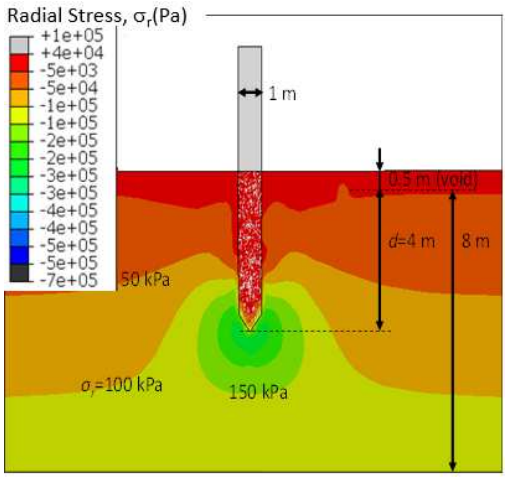

Figure 3. Radial total stresses for the penetration of a single rigid cylinder (d=4 m)

Maximum value of the radial stress at a certain depth (z) is achieved when the vibrator tip is at the same depth (d=z) (Figure 4). The peak value of radial stress is at the column wall when the tip of the vibrator is at an equal or lower depth than the one analysed $d \leq z$ and it moves further out of the column wall when the depth of the vibrator is higher than the one analysed $d > z$. These results agree well with the ones presenter by Bond and Jardine (1991) who already measured a steady increase in the radial total stress at a specific depth during pile penetration until the tip reached that depth, and a steady decrease as the pile tip advanced to greater depths.

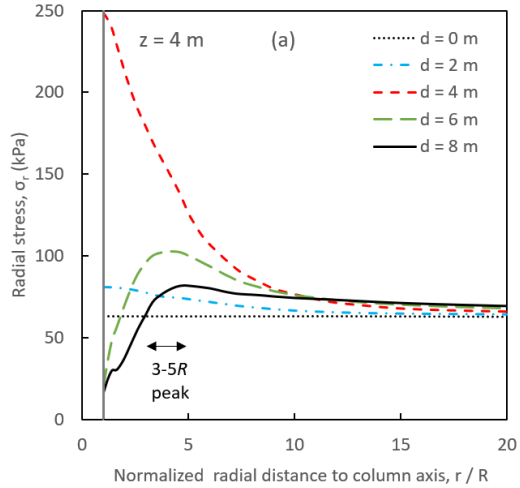

Figure 4. Radial total stresses with radial distance at several depths (d) for the penetration of a single rigid cylinder (z=4m)

In a similar way, the tangential stresses at a specific depth also reach a maximum when the tip is at this depth **Error! Reference source not found.**(Figure 5). When the cylinder tip further penetrates below the studied depth ($d > z$), the tangential stresses decrease, but just in the close vicinity (e.g., $r < 3R$). The more the cylinder penetrates, i.e. larger values of d, the larger the plastic annulus is at a specific depth and the more the peak of tangential stresses moves away from the cylinder wall. The elastic region ($r > 6R$), where the tangential stresses decrease, is clearly visible.

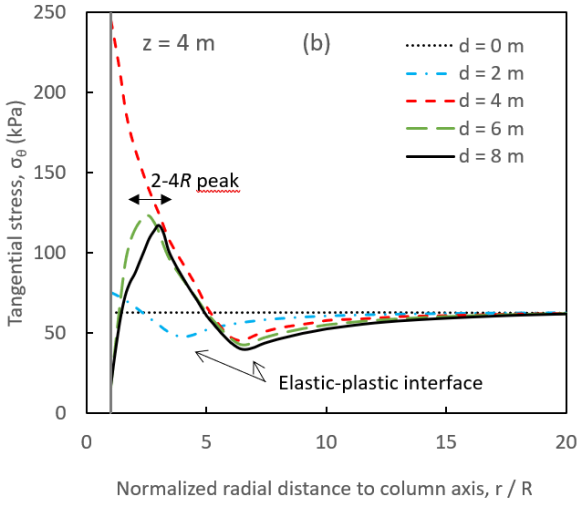

Figure 5. Tangential total stresses with radial distance at several depths (d) for the penetration of a single rigid cylinder (z= 4 m):

Values of vertical, radial and tangential stresses when d=z compare relatively well with the ones obtained using the cavity expansion solution (e.g., Baguelin et al. 1978) (Figure 6). The differences may be attributed to the non-plane strain conditions in the vertical direction due to the free surface modelled and the tip effects considered in the numerical simulations.

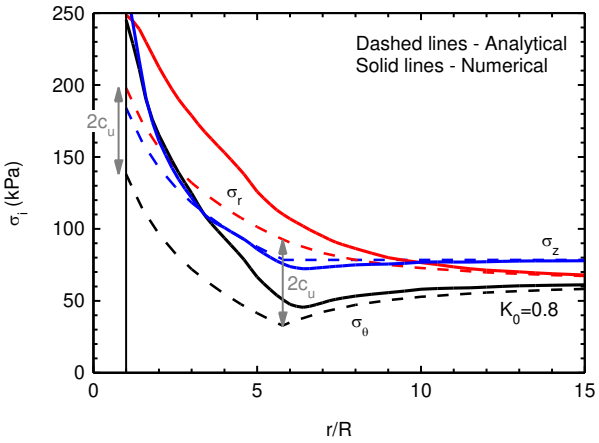

Figure 6. Comparison between numerical results of the installation of a single rigid cylinder (z=d=4m) with the analytical solution for cylindrical cavity expansion

3.2 *Installation of two columns*

When installing a second stone column close to a one already installed, the effects of the column installation interact as the area on influence (around 10R) is larger than the common spacings between columns (e.g., 1.5 to 3 m, which usually corresponds to 3-6 R) (e.g., Figure 7).

Radial stresses after the complete installation of both columns (full penetration of two rigid cylinders d=8m) at the depth of 4 meters are shown in Figure 8 and Figure 9. Figure 8 shows the results for the original position of

the columns (SC1 on left and SC2 on the right). For each installation the axis is placed at the centre of the column but for a better comparison, in Figure 9 the results have been plotted taking as the axis the centre of the last installed column, i.e., displacing 2 m (column spacing) to the left the results for SC2.

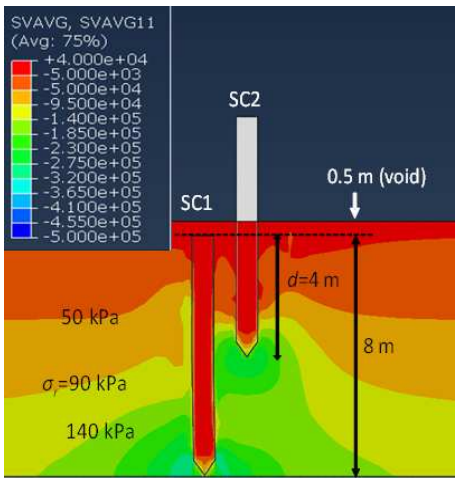

Figure 7. Radial total stresses for the penetration of a second rigid cylinder (d=4 m)

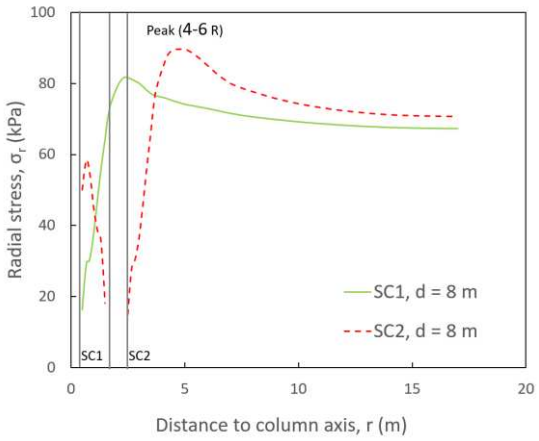

Figure 8. Radial stresses with radial distance for the penetration of two rigid cylinders (z=4m) (original position)

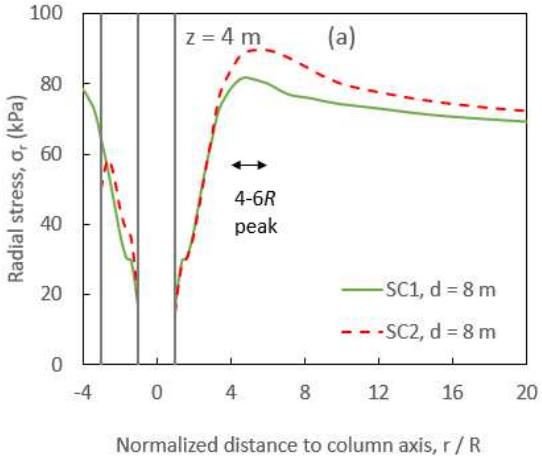

Figure 9. Radial stresses with radial distance for the penetration of two rigid cylinders (z=4m) (centred at the last installed column)

Results show that the peak of radial stress is higher after the installation of the second column and it is slightly further away from the column wall (Figure 9). Radial stresses close to the first column wall change when the second column is installed.

3.3 Installation of a group of 9 columns

Installation of a group of 9 columns with two different installations sequences: "Outside in" and "Inside out" (Figure 2Figure 2) have been modelled. A representative cross section is chosen to present the results (Figure 2) at a depth of 4 meters (*z*= 4 m). The cylindrical coordinate system is centred at the central column axis. Figure 10 presents the radial (horizontal in-plane), which further increases with the installation of more columns. The peak value is almost double in the case of "Outside in" than just after the installation of one single column which is approximately 80 kPa. For two columns the peak value is around 90 kPa. In the "Inside out" sequence it is slightly lower, as the value is around 135 kPa. The peak values are reached outside the column group, but close to the outer columns of the group, at a distance around 2-4*R*.

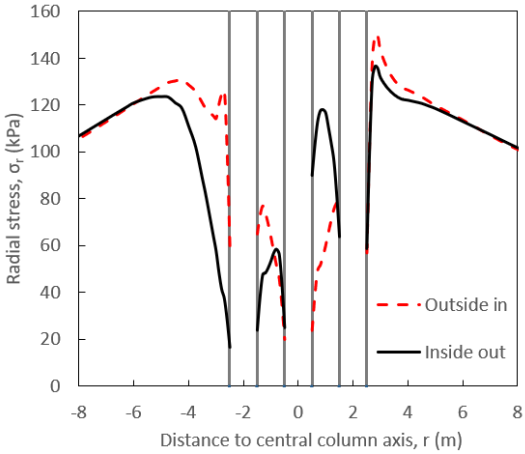

Figure 10. Radial stresses with radial distance at the reference cross-section for the penetration of nine rigid cylinders (z= 4 m)

Radial stress contours are presented in Figure 11 so the effect of each sequence can be appreciated. A better improved area surrounding the group of columns, i.e., larger radial stresses providing a better lateral confinement is achieved with the Outside in" sequence. Besides, the installation effects of the "Inside out" configuration are clearly not symmetric, which could later result in non-uniform settlements of a footing on top of the group of columns, even under centred loads.

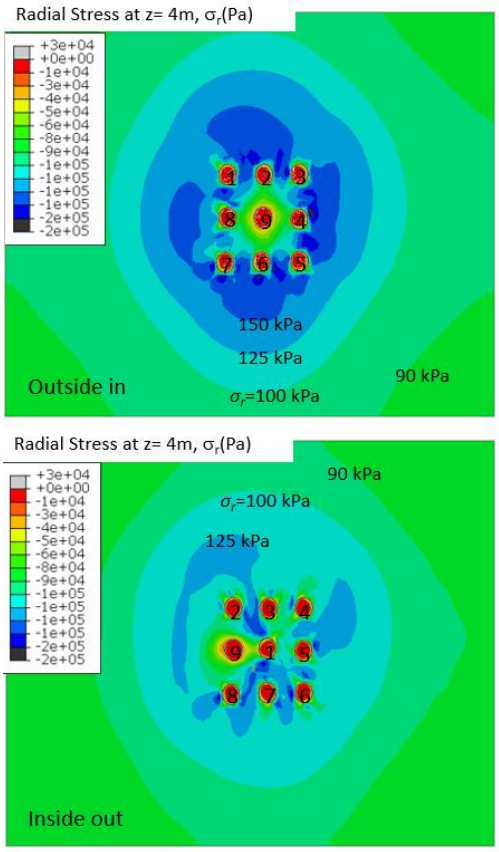

Figure 11.Radial total stress contours at z=4 m after the installation of a group of nine columns.

The excess pore pressures (Δu) have been estimated using Henkel's equation and the numerically simulated variations of total stresses:

$$\Delta u = \Delta\sigma_{oct} + 3a|\Delta\tau_{oct}| \quad (1)$$

where $\Delta\sigma_{oct}$ and $\Delta\tau_{oct}$ are the variations of octahedral normal and shear stresses, respectively, and a is the Henkel's a pore pressure parameter. The value of a is taken as 0.3 which corresponds to a Skempton's A pore pressure parameter of 0.75 (Table 1), and it is a common value for normally consolidated clays. Calculated excess pore pressures after the installation of the nine columns for both installation sequences in the reference cross section (Figure 2) are not very different (Figure 12).

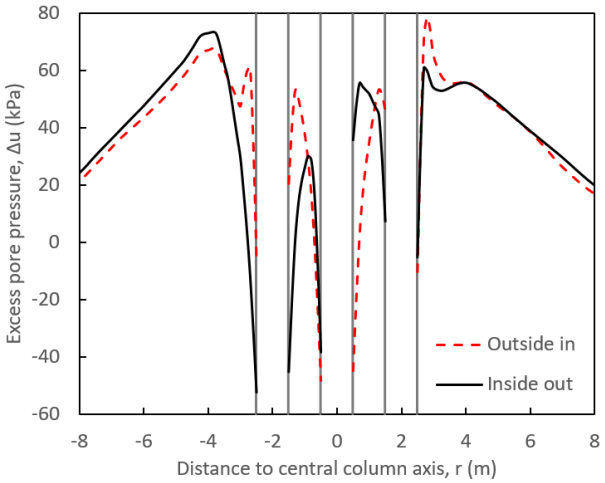

Figure 12. Excess pore pressures with radial distance for the penetration of nine rigid cylinders (z= 4 m)

Calculated values of excess pore pressures during the installation of the nine columns at the reference point at *z*= 4m, (*a* in Figure 2) are presented in (Figure 13). The horizontal axis represents the number of columns installed (e.g 1.5 indicated that the first columns has been already installed, but the tip of the second column is still at 4 meters depth, half way through). This representation allows to compare the results numerically obtained with readings taken in the field of piezometers located at a certain depth between columns during their installation. In this case, similar peak and final values of excess pore pressures are found for both installation sequences. The two highest peaks in both sequences correspond to the installation of two contiguous columns when the tip is at the same depth as the point (*z*=*d*= 4m) (e.g. SC1 and SC2 for the for "Outside in" and SC2 and SC3 for "Inside out"). Except in the case of the column installed just after the two contiguous columns, the excess pore water pressures are greater at the end of the column installations than at the beginning. In addition, excess pore pressures do not change when columns are installed outside the area of influence (plastic zone) in this case SC5 for "Outside in" and SC6 for "Inside out".

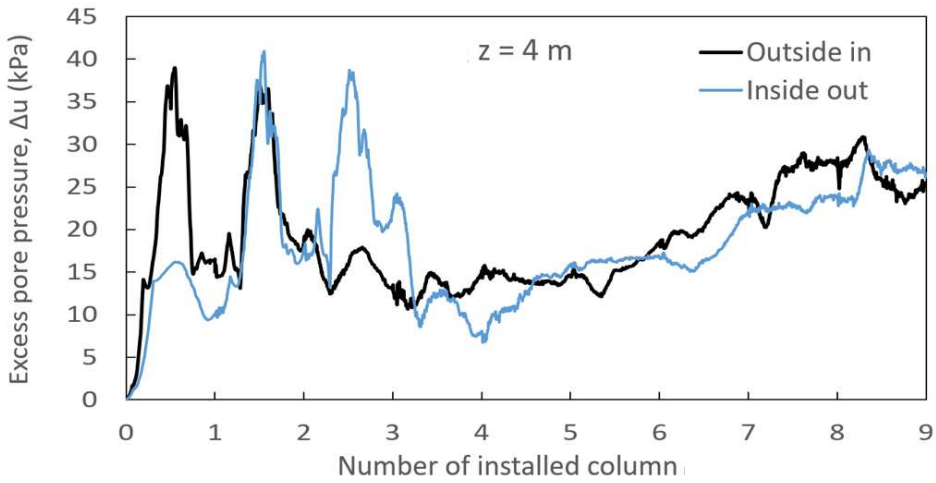

Figure 13. Excess pore pressures at the reference point (z=4m) during the penetration of the nine columns.

4 CONCLUSIONS

Results of simplified CEL finite elements simulations of the installation of a single column, two columns and a group of nine columns show the surrounding soil alteration with increased total stresses and pore water pressures. Aspects such as the dissipation of pore pressure or the gravel placement are not considered, and just and homogeneous purely cohesive soil layer with constant undrained shear strength has been analysed.

Installation effects interact between each other when two columns are installed at common spacings. The peak of radial horizontal stresses due to column installation is slightly higher than that for the installation of a single column and is located a bit further away from the column wall. The plastic annuli around the columns get larger than for a single column.

For a group of nine stone columns, the radial stresses further increase with the installation of more columns and the peak values are reached outside the column group, at a distance around 2-4R. Peak and final excess pore pressures calculated at the middle point between two columns are similar in the two studied installation sequences, namely "Outside in" and "Inside out". The excess pore pressures show a similar trend than the one registered in the field, peaks when the closest columns are being installed and the tip is at the studied depth, it drops as the column penetrates further and a gradual accumulation of excess pore pressures after the installation of each column is shown. Comparing both installation sequences, the "Outside in" generates slightly larger radial stresses surrounding the group of columns (providing a better lateral confinement) and the installation effects of the "Inside out" configuration are clearly not symmetric.

5 REFERENCES

Amoroso, S., Rollins, K.M., Monaco, P., Thorp, A. 2015. Use of SDMT testing for measuring soil densification by ground improvement in Christchurch. New Zealand. *3rd Int. Conf. Flat Dilatometer* DMT'15, 177–184.

Baguelin, F., Jézéquel, J.-F., Shields, D.H. 1978. The pressuremeter and foundation engineering. Trans Tech Publications: Clausthal, Germany

Barksdale, R.T., Bachus R.C. 1983. *Design and construction of stone columns*. Report FHWA/RD-83/026. Springfield: Nat. Tech. Information Service.

Castro, J., Karstunen, M. 2010. Numerical simulations of stone column installation. *Can. Geotech. J.* **47**(10), 1127-1138.

Castro, J., Sagaseta, C. 2012. Pore pressure during stone column installation. Proc. ICE - Ground improvement, 165(2), 97-109.

Farias, M.M., Nakai, T., Shahin, H.M., Pedroso, D.M., Passos, P.G.O., Hinokio, M. 2005. Ground densification due to sand compaction piles. *Soils Found*., 45, 167-180.

Geramian, A., Castro, J., Ghazavi, M., Miranda, M. 2022. Installation of groups of stone columns in clay: 3D Coupled Eulerian Lagrangian analyses. *Comput. Geotech.* **151**, 104931.

Han, J., 2015. *Principles and practices of ground improvement*. Wiley, Hoboken, New Jersey, USA.

Kirsch F. 2004. *Experimentelle und numerische Untersuchungen zum Tragverthalten von Rüttelstopfsäulengruppen*. Dissertation, Technische Universität Braunschweig.

Kirsch, K., Kirsch, F. 2010. *Ground Improvement by Deep Vibratory Methods*. Spon Press: London, UK.

McCabe, B.A., Kamrat-Pietraszewska, D., Egan, D. 2013. Ground heave induced by installing stone columns in clay soils. *Proc. ICE – Geotech. Eng*., 166, 589-593.

Nagula, S.S., Nguyen, D.M., Grabe, J. 2018. Numerical modelling and validation of geosynthetic encased columns in soft soils with installation effect. *Geotext. Geomembr.* **46**, 790–800.

Nguyen, H.H., Khabbaz, H., Fatahi, B. 2019. A numerical comparison of installation sequences of plain concrete rigid inclusions. *Comput. Geotech.* **105**, 1–26.

Pucker, T., Grabe, J. 2012. Numerical simulation of the installation process of full displacement piles. *Comput. Geotech.* **45**, 93-106.

Sexton, B.G., McCabe, B.A. 2015. Modeling stone column installation in an elastoviscoplastic soil. *Int. J. Geotech. Eng*. **9**, 500–512.

Soleimani, M., Weissenfels, C. 2021. Numerical simulation of pile installations in a hypoplastic framework using an SPH based method. *Comput. Geotech.* **133**, 104006.

Wang, J., Li, Q. 2019. Coupled continuum-discrete modelling of rammed floating stone column installation. *AIP Advances 9*, 015222.